Published online 17 April 2008

Nucleic Acids Research, 2008, Vol. 36, No. 8 ***2799–2810***
doi:10.1093/nar/gkn129

Structural probing of the HIV-1 polypurine tract RNA:DNA hybrid using classic nucleic acid ligands

Kevin B. Turner[1], Robert G. Brinson[2,3], Hye Young Yi-Brunozzi[3], Jason W. Rausch[3], Jennifer T. Miller[3], Stuart F. J. Le Grice[3], John P. Marino[2] and Daniele Fabris[1,*]

[1]University of Maryland Baltimore County, Baltimore, [2]Center for Advanced Research in Biotechnology of the University of Maryland Biotechnology Institute and the National Institute of Standards and Technology, Rockville and [3]HIV Drug Resistance Program, NCI, National Institutes of Health, Frederick, MD, USA

Received January 5, 2008; Revised February 22, 2008; Accepted March 9, 2008

ABSTRACT

The interactions of archetypical nucleic acid ligands with the HIV-1 polypurine tract (PPT) RNA:DNA hybrid, as well as analogous DNA:DNA, RNA:RNA and swapped hybrid substrates, were used to probe structural features of the PPT that contribute to its specific recognition and processing by reverse transcriptase (RT). Results from intercalative and groove-binding ligands indicate that the wild-type PPT hybrid does not contain any strikingly unique groove geometries and/or stacking arrangements that might contribute to the specificity of its interaction with RT. In contrast, neomycin bound preferentially and selectively to the PPT near the 5′$(rA)_4$:$(dT)_4$ tract and the 3′ PPT-U3 junction. Nuclear magnetic resonance data from a complex between HIV-1 RT and the PPT indicate RT contacts within the same regions highlighted on the PPT by neomycin. These observations, together with the fact that the sites are correctly spaced to allow interaction with residues in the ribonuclease H (RNase H) active site and thumb subdomain of the p66 RT subunit, suggest that despite the long cleft employed by RT to make contact with nucleic acids substrates, these sites provide discrete binding units working in concert to determine not only specific PPT recognition, but also its orientation on the hybrid structure.

INTRODUCTION

Converting single-stranded viral RNA into double-stranded DNA for integration is an essential step in HIV-1 replication mediated by reverse transcriptase (RT), a multifunctional enzyme performing both DNA polymerase and ribonuclease H (RNase H) activities (1,2). Initial polymerization of minus-strand DNA is primed by host-derived tRNA, whereas subsequent plus-strand synthesis requires viral primers defined as the 3′ and central polypurine tracts (PPTs) (3). These identical stretches of genomic RNA are not affected by template degradation associated with minus-strand synthesis. Instead, they are created by precise 3′-cleavage and eventually removed after plus-strand extension has been successfully initiated (1–3). Catalyzed by the RNase H function of RT, these hydrolytic events must be completed with high precision and specificity to produce proviral DNA of well-defined ends. The fact that imprecise PPT processing leads to impaired integration provides a powerful motivation for investigating the structural determinants of RNase H activity as potential targets for new antiviral strategies (4–6).

In vitro studies have demonstrated that single-base substitutions induce only minor variations in the PPT cleavage pattern, suggesting that its structure is recognized as a whole by RT (7–10). High-resolution structural analysis has been reported for RNA:DNA duplexes covering different sections of the PPT sequence and contiguous regions (Figure 1), revealing significant deviations from typical hybrid structures with intermediate characteristics between canonical A- and B-type double helices (11–14). In particular, an octamer spanning the junction between PPT and the adjacent unique 3′ (U3) sequence has shown a wide major groove approaching B-type dimensions and a bend of ~13° centered around the PPT-U3 cleavage junction (15). Constructs comprising the rA:dT tracts located 5′ of the cleavage site exhibited a significantly narrower minor groove than in typical hybrids (16). Minor groove compression was also observed in the crystal structure of a complex between

*To whom correspondence should be addressed. Tel: +1 410 455 3053; Fax: +1 410 455 2608; Email: fabris@umbc.edu
Correspondence may also be addressed to John P. Marino. Tel: +1 240 314 6160; Fax: +1 240 314 6255; Email: marino@umbi.umd.edu

The authors wish it to be known that, in their opinion, the first two authors should be regarded as joint First Authors

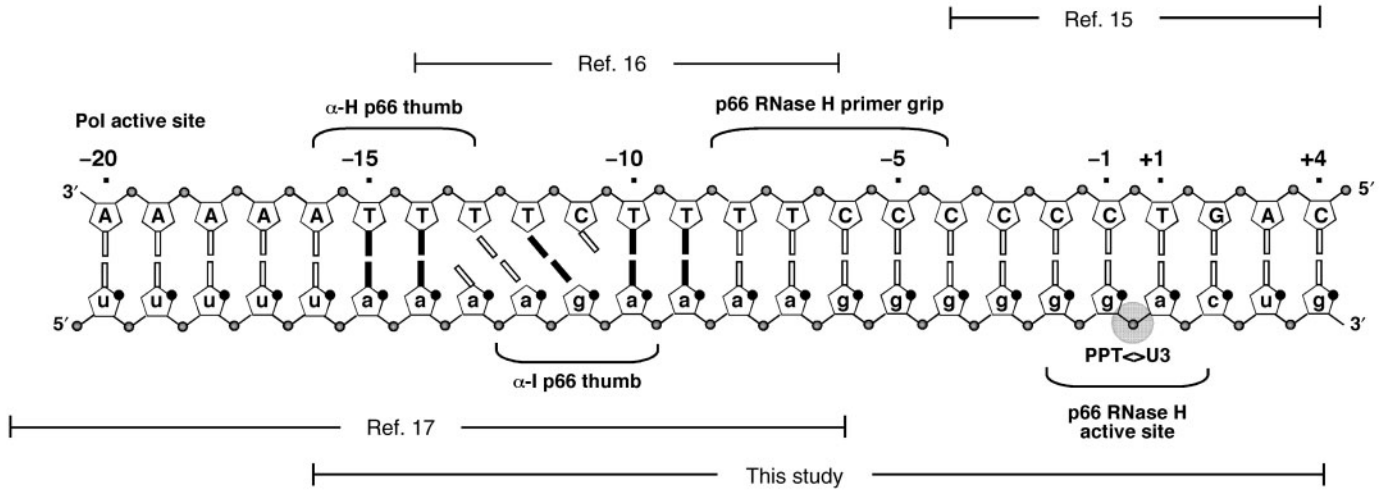

Figure 1. PPT-containing RNA:DNA hybrid. Indicated are regions for which high-resolution structures are available and their relationship with the sequence employed in this study.

RT and a RNA:DNA substrate extending farther upstream (17), which also displayed an unusual pattern of weakly paired, unpaired and mispaired bases (Figure 1). Chemical probing experiments performed in the absence of protein demonstrated that these pairing anomalies constitute an intrinsic characteristic of the PPT and not the direct result of RT binding (18). The hypothesis that these unique structural features may serve as specific recognition sites prompted further studies to determine the effects of base-pairing and substrate geometry on PPT cleavage specificity, which enabled mapping of motifs necessary for proper positioning of the RNase H catalytic site onto the PPT-U3 junction (Figure 1) (19–23).

In this report, the interactions between non-covalent probes selected from different classes of nucleic acid binders and a series of PPT substrates were assessed using direct infusion electrospray ionization (ESI) (24,25) and Fourier transform ion cyclotron resonance (FTICR) (26,27) mass spectrometry. Taking advantage of the inherently low energy afforded by this ionization technique to assess the stoichiometry and binding affinity provided by small molecule ligands (28–30), we recently probed the specific interactions between the nucleocapsid (NC) domain of Gag and isolated RNA stemloops of the HIV-1 packaging signal (31,32). We have now implemented this approach to evaluate the ability of archetypical ligands to form stable complexes with PPT, determine their binding modes and identify their specific sites on the duplex structure. Selected interactions were further investigated using high-resolution nuclear magnetic resonance (NMR) spectroscopy to confirm the stoichiometry and position of putative binding sites. Isothermal titration calorimetry (ITC) was finally employed to assess the stability of different PPT complexes and obtain the thermodynamic characteristics of their binding equilibria. The observed interactions are discussed in the context of structural features of the PPT that may guide selective RT processing to create the plus-stand primer from within the viral RNA genome.

MATERIALS AND METHODS

PPT substrates

All ribo- and deoxyribonucleotide phosphoramidites were purchased from Glen Research Corporation (Sterling, VA, USA). Oligonucleotides (20-mers) of DNA and RNA were synthesized using standard phosphoramidite chemistry on a PE Biosystems Expedite 8909 nucleic acid synthesizer. The individual strands were purified using preparative polyacrylamide gel electrophoresis (PAGE), dialyzed against sterile ddH_2O, then against either ESI (100 mM ammonium acetate, pH 7.0) or NMR buffer (80 mM NaCl, 10 mM phosphate, pH 7.0), and finally quantified with a UV–Vis spectrophotometer (260 nm). The single strands were finally annealed by mixing equimolar amounts of the desired constructs, heating the solution to 90°C for 3 min, and allowing the samples to slow-cool to form the duplex.

Mass spectrometry

All analyses were performed on a Bruker Daltonics (Billerica, MA, USA) Apex III FTICR mass spectrometer equipped with a 7T actively shielded superconducting magnet and a nano-ESI source built in-house. Desolvation temperature, skimmer voltage and other source parameters were optimized to allow for the observation of intact RNA non-covalent complexes, as previously described (31–34). Analyte solutions were mixed with iso-propanol immediately before analysis to a final concentration of 10% in volume to assist desolvation. Typically, 5 μl samples were loaded into the nano-ESI needle and a spray voltage of <1 kV was applied to the solution through a stainless steel wire inserted in the needle's back end. No solvent pumps were necessary, as the solution flow-rate was dictated by the applied voltage and the size of the nano-ESI needle tip (typically ~1–2 μm). Spectra were acquired in negative ionization mode and processed using XMASS 7.0.2 (Bruker Daltonics, Billerica, MA, USA). Scans were completed in broadband mode that allowed for a typical

150 000 resolving power at m/z 2000. The spectra were externally calibrated using a 1 mg/ml solution of CsI, which produced a series of peaks throughout the mass range of 1000–6000 m/z and enabled to achieve a typical mass accuracy of 20 p.p.m. or better across the range. Each analysis was performed a minimum of three times and only representative spectra were shown.

In tandem MS experiments, the precursor ion of interest was isolated in the FTICR cell using correlated RF sweeps (CHEF) (35) and then activated through sustained off-resonance irradiation–collision-induced dissociation (SORI–CID) (36). Frequency offsets below and above the resonant frequency of the precursor ion were sampled to avoid possible 'blind spots' in the product spectra. Best results were achieved by using irradiation frequencies that were 600–2000 Hz below that of the precursor ion. Typical activation regimes were reached by applying off-resonant pulses for 250 ms, using 26–31 dB attenuation of the maximum power output allowed by the hardware. Argon was used as the collision gas in pulsed bursts of 100–250 ms, which resulted in momentary increases from 1×10^{-11} to 1×10^{-7} mbar of the background pressure measured by the instrument gauge located underneath the ion optics. No attempt was made to determine the actual pressure within the FTICR cell.

NMR analysis

HIV-1 wild-type single-stranded RNA and DNA oligonucleotides were prepared and annealed as described above. The duplex was dialyzed against 80 mM NaCl and 10 mM NaH_2PO_4/Na_2HPO_4 at pH 7.0. Final duplex concentration was 225 μM (61.9 nmol). Neomycin B was titrated in 0.25 equivalents (15.5 nmol) up to a total of 2.0 equivalents (123.8 nmol). After each addition, the complex was equilibrated for 20 min before the ^{1}H NMR was acquired. RNase H-deficient mutant RT (E478Q RT) was prepared as described (37). The E478Q RT:PPT_{wt} complex was formed before final dialysis by mixing 11 nmol of each. The complex was then dialyzed into phosphate buffer using an Amicon Ultra-4 (MWCO 3000) centricon (Millipore, Billerica, MA). Final glycerol concentration was ~8%, and final complex concentration was ~40 μM. One-dimensional ^{1}H NMR data were acquired using a Bruker Biospin DMX600, equipped with a triple resonance, triple axis pulsed field-shielded gradient TXI HCN cryoprobe. Titrations of PPT substrate with neomycin B and RT were carried out at 10°C and 30°C, respectively, based on optimal temperatures found for observing the spectra of each complex. All 1D spectra were processed with (TopSpin software, Bruker Biospin, Billerica, MA, USA).

Isothermal titration calorimetry

HIV-1 wild-type PPT duplex was dialyzed in 80 mM or 240 mM NaCl and 10 mM NaH_2PO_4/Na_2HPO_4 at pH 7.0. Separate solutions of neomycin B were prepared using the same buffers. ITC experiments were performed at 30°C on a MicroCal VP-ITC (MicroCal, Inc., Northhampton, MA, USA). In a typical experiment, 5 μl aliquots of 800 μM neomycin B were injected from a 275 μl rotating syringe (313 r.p.m.) into an isothermal chamber containing 1.42 ml of 20 μM HIV wild-type PPT duplex. The initial delay before the first injection was 180 s. The duration of each 5 μl injection was 10 s with 240 s delay between each injection. The corresponding control experiment was also run in which neomycin B was injected into each buffer alone to take into account the heats of dilution. Each injection generated a heat burst curve (microcalories per second versus seconds) that was integrated using (Origin 5.0 software, Silverdale Scientific, Buckinghamshire, UK) to obtain the heat associated with each injection. After the heats of dilution were subtracted, the results were plotted (kilocalories/mole of injection versus molar ratio). The plot was fit with a model of either one set or two sets of equivalent sites using the Origin 5.0 software.

RESULTS AND DISCUSSION

Nucleic acid ligands with well-characterized binding modes can serve as non-covalent probes for assaying the ability of target substrates to sustain specific interactions and for identifying the structural features necessary for stable binding (31,32). For this purpose, ligands employed here were selected among general intercalators (ethidium bromide), minor groove binders (distamycin A), mixed-mode intercalator/minor groove binders (mitoxantrone) and multifunctional polycationic aminoglycosides (neomycin B) (Scheme 1) (38–40). The extensive knowledge of the chemical properties of these ligands, as well as their binding preferences, allows for valid conclusions on the specific nature of target substrates. The effects of helical structure and pairing anomalies on binding mode were investigated by employing not only a consensus PPT RNA:DNA hybrid (PPT_{wt}, Scheme 2), but also constructs in which both strands consisted exclusively of ribo- or deoxyribonucleotides (PPT_{RNA} and PPT_{DNA}, respectively). A control hybrid duplex designated PPT_{swp} was also included in which the DNA and RNA sequences were interchanged (Scheme 2).

PPT-ligand binding modes

The formation of non-covalent complexes between selected binders and PPT constructs was monitored directly by high-resolution mass spectrometry to provide unambiguous information about the composition and stoichiometry of any species at equilibrium in solution. Reversing established multiplexed strategies in which groups of ligands are presented together to a single target in solution (31,41,42), we treated equimolar mixtures of the four PPT constructs with each individual probe to directly compare binding specificity. This approach promotes competition among substrates and yields distinctive assembly distributions that reflect the strength of the respective interactions. Due to the similar charging properties of the various species in the mixture, signal intensities correlate well with relative abundances in solution, which can be readily translated into relative scales of binding affinities (see Materials and methods section).

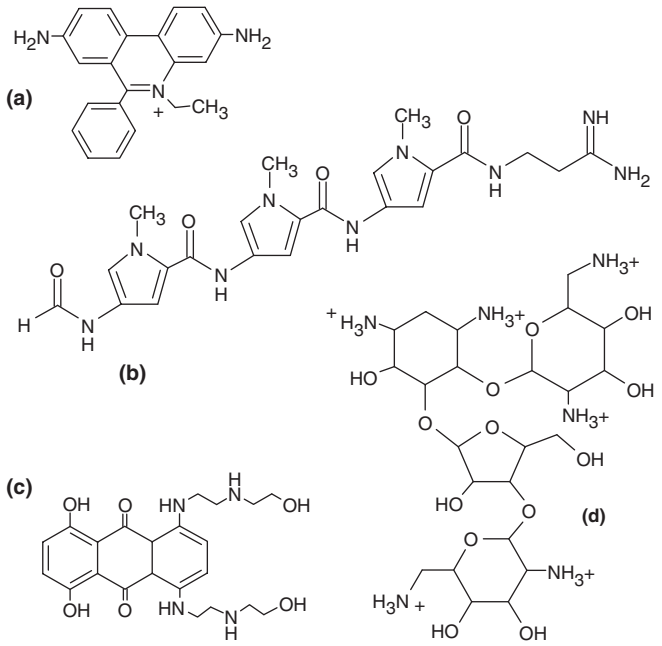

Scheme 1. Archetypical nucleic acid ligands used as non-covalent probes in this study: (**a**) ethidium bromide, representative of base intercalators; (**b**) distamycin A, a typical minor-groove binder; (**c**) mitoxantrone, a mixed-mode intercalator/groove binder; and (**d**) neomycin B, a polycationic aminoglycoside.

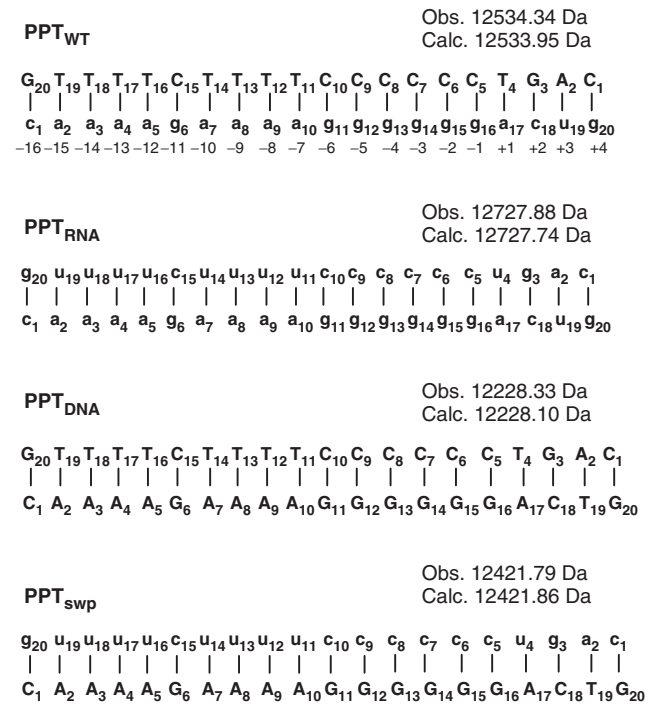

Scheme 2. PPT-containing duplexes. PPT_{wt}: wild-type hybrid from HIV-1 subtype A; PPT_{RNA}: both strands made of RNA; PPT_{DNA}: both strands DNA; PPT_{swp}: sequences of the RNA and DNA strands swapped. Sequences are numbered from 5′ to 3′, and biological numbering relative to the scissile −1g/+1a phosphodiester bond is indicated. Nucleotides in uppercase denote DNA, and lowercase denotes RNA. The monoisotopic mass observed by nanospray-FTICR for each duplex construct is reported together with the respective mass calculated from sequence (see Materials and methods section).

A representative competition experiment is shown here by the titration of a solution containing 5 μM of each PPT substrate with the mixed-mode binder mitoxantrone (Figure 2). ESI-FTICR analysis of the initial mixture provided fully resolved signals for all four substrates, together with typical cation adducts observed in nucleic acid analysis (Figure 2a). Non-covalent assemblies containing up to three ligand units were readily detected for each duplex after addition of one equivalent of mitoxantrone per substrate (Figure 2b, see Materials and methods section). In a clear concentration-dependent fashion, larger amounts of ligand induced the binding of additional units and increased the ratio between bound and free substrates in solution. When a 10-fold excess was added, the PPT_{DNA} construct bound five mitoxantrone equivalents, whereas the other substrates provided a maximum binding of only four units (Figure 2c). While the available sites were progressively occupied during the titration, binding of one ligand did not appear to facilitate or hamper that of the next, suggesting that the sites are independent and cooperative effects are insignificant. The patterns of assembly formation and substrate consumption are consistent with the following relative scale of binding affinities: $PPT_{DNA} > PPT_{wt} \approx PPT_{RNA} \approx PPT_{swp}$.

Analyzed in identical fashion, each class of binders formed stable complexes with distinctive binding modes. As summarized in Table 1, ethidium bromide displayed a scale of relative binding affinities matching that of mitoxantrone, as expected from their similar intercalating activities. Both molecules provided significantly higher stoichiometries than the remaining non-covalent probes in the study, consistent with their ability to insert into multiple positions of the double-stranded PPT structure. The preference manifested by these binders for PPT_{DNA} can be ascribed to the tighter nature of base stacking in canonical B-type helices than in either canonical A-type or hybrid structures, which accounts for greater stabilization of intercalating interactions. The maximum stoichiometry obtained from these molecules (Figure 3a) matches the presence of five possible sites between adjacent GC pairs, which are particularly favorable to intercalation (43,44). The fact that only four units bound to the other PPT constructs is consistent with more limited stabilization afforded by the less-extensive stacking of A-type and hybrid double helices.

The minor groove binder distamycin A also manifested an overall preference for PPT_{DNA}, but displayed lower overall stoichiometries (Table 1). In this case, the relative scale of binding affinities reflects the increasing size of the minor groove in the PPT series, with hybrid structures exhibiting intermediate properties between the more favorable narrow groove of the B-type DNA duplex and the wider A-type RNA (12,15). This class of oligopeptide molecules binds preferentially to sites that include four or five consecutive AT base pairs, establishing H-bonds with the N3-adenine and O2-thymine (45). For this reason, the two $(dA)_4$:$(dT)_4$ tracts in the 5′ region of the DNA duplex are likely responsible for the tight binding of the first two units (Figure 3b). The third molecule required to account for the observed stoichiometry could enjoy

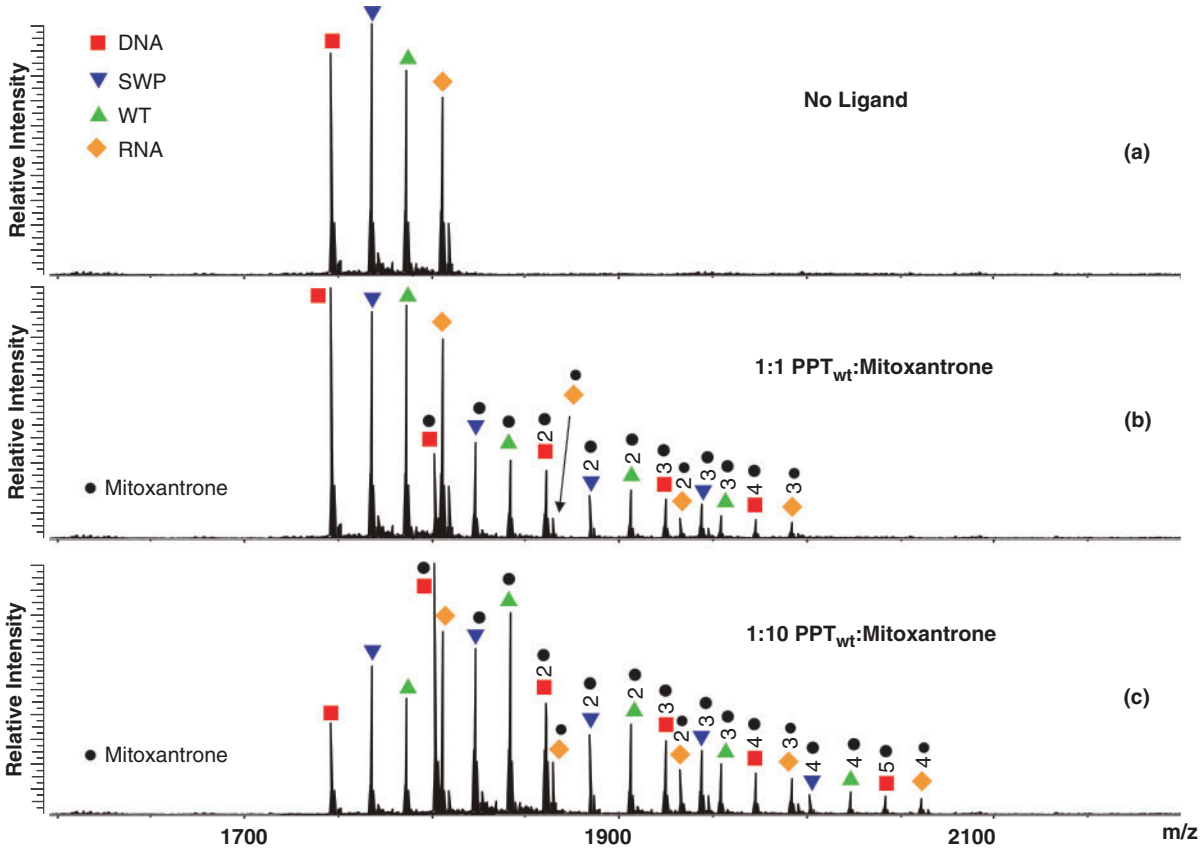

Figure 2. Nanospray-FTICR mass spectra of: (**a**) the initial equimolar mixture of the four PPT substrates (5 μM each); (**b**) the products obtained after a 1-fold per substrate addition of the mixed-mode binder mitoxantrone; (**c**) the assemblies after 10-fold ligand addition (see Materials and methods section). Red filled square: PPT_{DNA}; orange filled diamond: PPT_{RNA}; green filled triangle: PPT_{wt}; blue filled inverted triangle: PPT_{sw} and black filled circle: bound ligand. The high resolution and accuracy afforded by this analytical platform enabled unambiguous identification of the different species in solution according to their unique molecular masses (see also Scheme 2).

Table 1. Summary of the stoichiometries and relative binding affinities obtained by titrating an equimolar mixture of the four PPT substrates with increasing amounts of each individual ligand (see Materials and methods section)

Ligand	PPT_{wt}	PPT_{swp}	PPT_{DNA}	PPT_{RNA}	Relative affinity
Ethidium bromide (units bound)	4	4	5	4	DNA>WT≈RNA≈Swp
Mitoxantrone (units bound)	4	4	5	4	DNA>WT≈RNA≈Swp
Distamycin A (units bound)	2	2	3	1	DNA>WT>Swp>RNA
Neomycin B (units bound)	2	1	1	1	WT>RNA>Swp>DNA

The reported stoichiometry corresponds to the maximum number of units observed upon 10-fold addition of ligand over the total amount of each duplex substrate in solution.

only weaker stabilization from specific interactions with the non-consecutive AT pairs at the 3′-end of the construct (Scheme 2). Considering the overall unfavorable situation afforded by the minor groove of double-stranded RNA, it was not surprising that PPT_{RNA} bound only one equivalent within the range of concentrations covered by the titration experiments (Figure 3b).

Unique among the probes used in the study, the aminoglycoside neomycin B exhibited its highest relative affinity for the wild-type RNA:DNA PPT, while PPT_{DNA} fell to the bottom of the scale (Figure 3c and Table 1). This class of molecules has a pronounced ability to interact with motifs that disrupt regular double-helical pattern, including non-canonical pairs, platforms, bulges, bends and other anomalies (46). These peculiar features can provide unique H-bonding opportunities for the amino groups of aminoglycosides, which are placed in optimal positions by the flexible 2-deoxystreptamine scaffold (46). In addition, electrostatic interactions between protonated amino groups on the aminoglycoside molecule and highly electronegative areas on the motif surface contribute to further stabilize binding of this class of ligands (31,32,46). The fact that PPT_{wt} displayed the highest affinity in the substrate series suggests that unusual structural characteristics set it apart from the canonic helical structures of PPT_{RNA} and PPT_{DNA}. These favorable features require

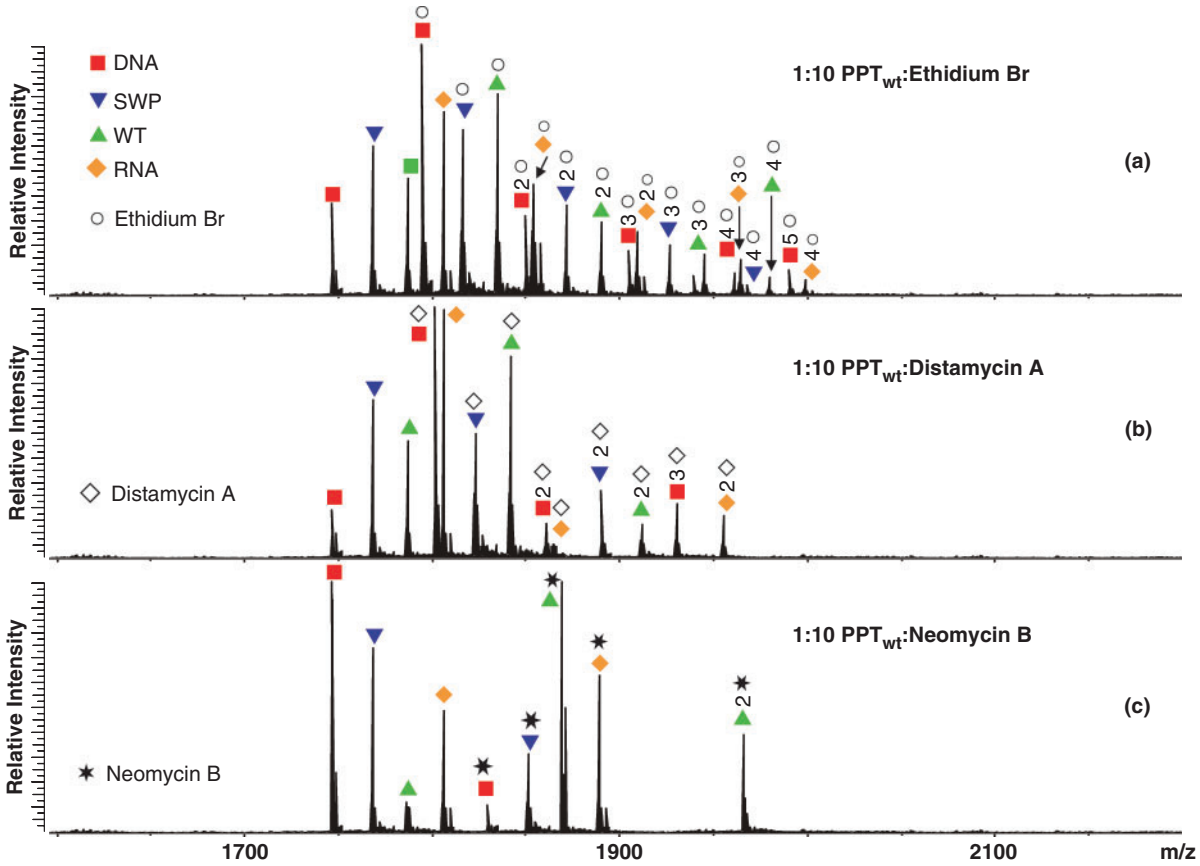

Figure 3. Nanospray-FTICR mass spectra of the initial equimolar mixture of the four PPT substrates (5 μM each) after a 10-fold per substrate addition of: (**a**) ethidium bromide; (**b**) distamycin A; (**c**) neomycin B (see Materials and methods section). Red filled square: PPT_{DNA}; orange filled diamond: PPT_{RNA}; green filled triangle: PPT_{wt}; blue filled inverted triangle: PPT_{sw}; open circle: ethidium; open diamond: distamycin A; and asterisk: neomycin B.

that the PPT be coded in the RNA strand of the hybrid duplex, as indicated by the significantly lower affinity of the sequence-swapped construct PPT_{swp}, in which the PPT is present in the DNA strand (Figure 3c). The fact that neomycin B provided the lowest stoichiometry and highest affinity in the ligand series while competing for the PPT_{wt} substrate further indicates the unique character of the structures involved in these specific interactions.

PPT-aminoglycoside binding sites

The presence of multiple basic groups on a flexible 2-deoxystreptamine scaffold makes the nature of aminoglycoside binding very similar to that of basic peptides (Scheme 1) (46). In fact, nucleic acid motifs that are specifically recognized by aminoglycosides also have a strong tendency to favor stable protein interactions (32). For this reason, mapping the specific binding sites of neomycin B on the wild-type RNA:DNA hybrid could provide important information on the RT-PPT recognition mechanism. This was addressed by combining tandem mass spectrometry (MS/MS) and NMR spectroscopy. The former approach involves isolating the precursor ion of interest within the FTICR cell, submitting it to low-energy collisions with target gas, and analyzing the fragments produced by the dissociation process, which are characteristic of the precursor composition and chemical structure (47,48). We recently reported that the fragmentation patterns obtained from intact ligand–RNA complexes contain series of sequence ions with distinctive gaps corresponding to the nucleotides involved in ligand interactions (32). This gas-phase footprinting technique successfully localized the aminoglycoside sites on different stem-loop domains of the HIV-1 packaging signal, correlating their location with the position of known contacts between these structures and the viral nucleocapsid protein.

When applied to the PPT_{wt} RNA:DNA hybrid binding a single neomycin B, MS/MS provided ion series consistent with fragmentation of both strands (Figure 4). Importantly, protection effects induced by the ligand inhibited the fragmentation of nucleotides located across the PPT-U3 junction, identifying this biologically-critical region as one of the specific binding sites. When the assembly containing two units of neomycin B was analyzed, the characteristic ion series provided *two* distinctive gaps in their regular patterns, with the first matching the PPT-U3 junction and the second corresponding to nucleotides located around the 5′ $(rA)_4$:$(dT)_4$ tract at the opposite end of the hybrid (Figure 5). The regions of protection are in good agreement with binding sites of the RNase H active site and thumb subdomain of the p66 RT subunit in the RT•PPT complex (Figure 1).

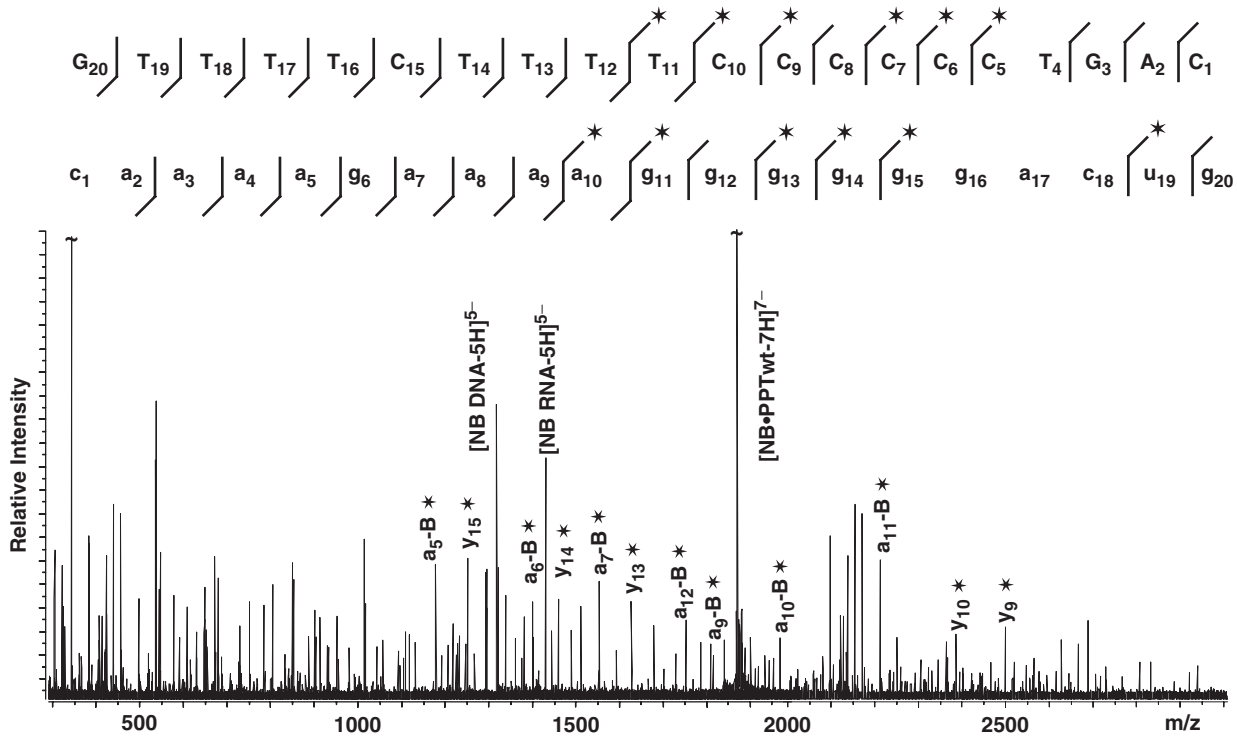

Figure 4. Tandem mass spectrum of the non-covalent 1:1 PPT_{wt}:neomycin B complex (observed mass 13148.74 Da, calculated from sequence 13148.26 Da, see Materials and methods section). For clarity, only some of the characteristic ion series are labeled on the spectrum, which contain either the 5′- or 3′-end (e.g. a_x-B and y_x, with x indicating the numeration from the respective end; $-B$ indicates the loss of nucleobase at the site of cleavage). The asterisk symbol identifies products containing noncovalently bound neomycin B. All product ions observed for the DNA and RNA strands that constitute the substrate are reported on the respective sequences to highlight nucleotides prevented from undergoing fragmentation in the presence of bound ligand (32). The lines mark the phosphodiester bond cleaved by the gas-phase dissociation processes, pointing toward the respective end included in each fragment; asterisk indicates products containing noncovalently bound neomycin B. A clear gap in the fragmentation pattern exhibited by the DNA and RNA strands identifies the position of protected nucleotides.

It is important to note that the results provided by the complex with one ligand did not display any sign of protection at, or around, the 5′ $(rA)_4$:$(dT)_4$ tract. Therefore, the absence of alternative populations in which either site may be individually occupied indicates that the PPT-U3 junction possesses significantly higher affinity than the 5′ $(rA)_4$:$(dT)_4$ tract and that the latter is occupied only after the former is saturated. This interpretation is supported by electrostatic surfaces generated by Delphi (49) from the high-resolution coordinates obtained in refs. (15,17), which show very distinctive electronegative patches located at the PPT-U3 junction and 5′ $(rA)_4$:$(dT)_4$ tract, with the former providing a higher density. It is also consistent with the recognition of the RNase domain of RT at the PPT-U3 junction through primarily electrostatic interactions with the phosphodiester backbone of the PPT substrate.

Further insights into the position of the specific binding sites were revealed by high-resolution ^1H NMR. Ligand binding to the wild-type PPT was followed by monitoring changes in the imino proton spectrum of PPT_{wt} upon titration with neomycin B in increments of 0.25 equivalents to a final 2:1 ligand:substrate ratio (Figure 6a). The imino proton chemical shift assignments are indicated for the free PPT_{wt} and were determined using 2D NOESY spectra (50). Upon addition of neomycin B to PPT_{wt}, perturbations are observed for a subset of imino proton resonances. After addition of one equivalent of ligand, a shift in the imino proton signals was detected for g(−1), T(+1) and G(+2) (indicated by the arrows), consistent with selective binding at the PPT-U3 junction. In addition, uniformly subtle downfield shifts were observed for imino protons assigned to the G-tract 5′ of the PPT-U3 junction, which further localizes binding of neomycin B to this end of the PPT. After the primary site was saturated, addition of a second equivalent did not introduce any detectable shift of the imino protons, but caused only a broadening of their signals. This behavior is typical of intermediate chemical exchange processes on the NMR timescale and is suggestive of a weaker, more non-specific binding interaction(s) between ligand and PPT substrate. While the NMR data does not allow mapping of this secondary site(s), the observation of consecutive binding events in the NMR titrations is consistent with the observation of high and low affinity sites in the ESI-FTICR experiments.

In order to validate the relevance of using small molecule ligands as probes for understanding how HIV-1 RT may interact with its PPT substrate, we have acquired NMR data on a HIV-1 RT•PPT complex, which could be compared with those obtained from PPT upon aminoglycoside binding (Figure 6b). As with neomycin, binding of an RNase H-deficient mutant RT (E478Q RT) to the wild-type PPT was followed by monitoring changes in the imino proton spectrum of PPT_{wt} upon titrating one

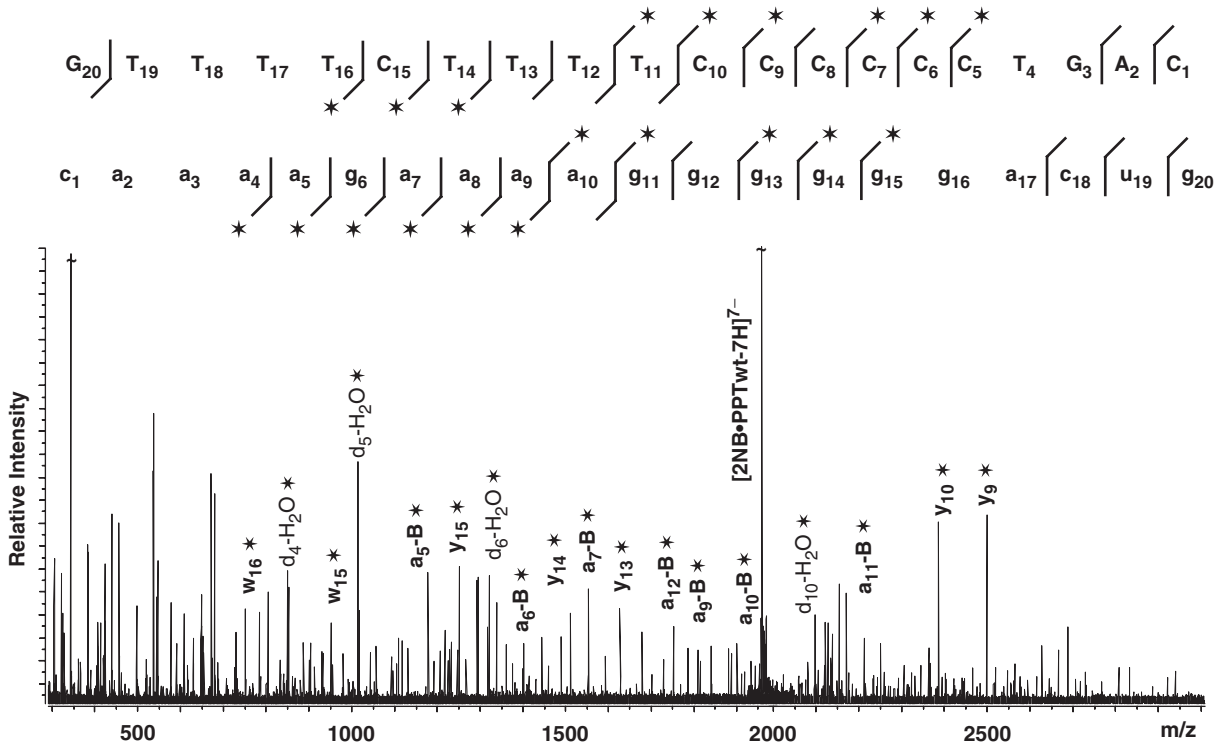

Figure 5. Tandem mass spectrum of the non-covalent 1:2 PPT_{wt}:neomycin B complex (observed mass 13762.43 Da, calculated from sequence 13762.57 Da, see Materials and methods section). For clarity, only some of the characteristic ion series are labeled on the spectrum, which contain either the 5′- or 3′-end (e.g. a_x−B and y_x, with x indicating the numeration from the respective end; −B indicates the loss of nucleobase at the site of cleavage). The asterisk symbol identifies products containing non-covalently bound neomycin B. All product ions observed for the DNA and RNA strands that constitute the substrate are reported on the respective sequences to highlight nucleotides prevented from undergoing fragmentation in the presence of bound ligand (32). The lines mark the phosphodiester bond cleaved by the gas-phase dissociation processes, pointing toward the respective end included in each fragment; asterisk indicates products containing noncovalently bound neomycin B. In this case, two distinct gaps are evident in the ion series observed for the DNA and RNA components of the construct, thus revealing the presence of two separate binding sites.

equivalent of RT (Figure 6b). In previous studies, this RNase H-deficient mutant RT has been shown to bind to a number of different short RNA:DNA hybrid sequences with low nanomolar affinities that exceed the affinity observed for wild-type RT (51,52). In addition, single molecule fluorescence spectroscopy has shown that RT binds with a 1:1 stoichiometry to PPT substrates comprising the same sequences used in this study, and that it overwhelmingly adopts a configuration with the RNase H domain over the PPT/U3 junction (53).

In the NMR experiment, formation of the complex between RT and PPT_{wt}, results in general broadening of the imino proton signals from the PPT_{wt} as would be expected based on the large size of the complex (MW > 130 kDa) when compared to the PPT_{wt} substrate (MW ~ 14 kDa). Nonetheless, more significant broadening is observed for a selective subset of imino proton resonances that is consistent with direct contacts between RT and the 5′ $(rA)_4$:$(dT)_4$ tract and the PPT-U3 junction. Uniformly subtle downfield shifts are also observed for imino proton resonances assigned to the G-tract 5′ of the PPT-U3 junction, which further indicates RT contacts at this end of the PPT. While the broadness of the imino spectrum of the RT•PPT complex only allows a low-resolution analysis at this time, the qualitative observation that the addition of RT selectively perturbs a subset of imino resonances that is similar to those affected by binding of neomycin B suggests that common regions of the PPT may be contacted in both cases. The fact that the perturbations to the spectra are not identical in the two experiments is not surprising considering that the chemical nature of the neomycin B versus RT contacts with the PPT are likely very different. Nonetheless, the RT•PPT data support the general premise that neomycin B highlights uniquely structured sites along the PPT that appear to coincide with contact points for protein binding. We would also note that the RT•PPT spectra we have obtained are the only ones to date analyzing this HIV nucleoprotein complex.

Thermodynamics of PPT_{wt}—neomycin B binding

Since neomycin B showed specific binding to the same regions of the wild-type PPT RNA:DNA hybrid, we next investigated the thermodynamic characteristics of these interactions. ITC allows determination of association constants and other thermodynamic parameters of binding equilibria involving both protein (54) and nucleic acid (55) substrates. For this reason, titration of PPT_{wt} with neomycin B was followed by ITC in solutions of different salt content (i.e. 80 mM and 240 mM NaCl) to modulate the strength of electrostatic interactions and discriminate against possible non-specific binding.

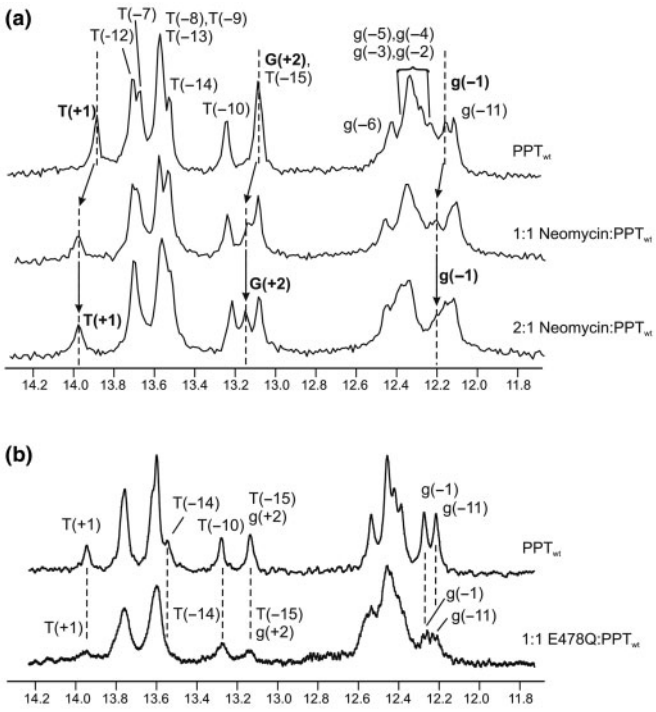

Figure 6. One-dimensional water flip-back watergate ^{1}H NMR spectra of the imino region of the PPT_{wt} duplex after titration with neomycin B at 10°C, or E478Q RT at 30°C, in 80 mM NaCl and 10 mM NaH_2PO_4/Na_2HPO_4 at pH 7.0. (**a**) For the neomycin titration, the concentration of the PPT_{wt} duplex was ~200 μM. 1D ^{1}H NMR spectra are shown in the absence (upper trace) and presence of 1.0 equivalents (middle trace) and 2.0 equivalents (lower trace) of neomycin B. The imino resonances for G(+2), T(+1), and g(−1) where chemical shift changes can be tracked are highlighted in bold. Dotted lines and arrows indicate the shift in position of the resonances. (**b**) For the E478Q RT titration, the concentration of PPT_{wt} was ~40 μM. 1D ^{1}H NMR spectra are shown for PPT_{wt} in the absence (upper trace) and presence of 1.0 equivalent (lower trace) of E478Q RT. Imino protons were assigned using 2D NOESY experiments; assignments are listed above each peak.

The ITC profiles at both ionic strengths are shown in Figure 7a and c. Each peak corresponds to a single 5.0 μl injection of ligand (see Materials and methods section), which was subsequently integrated to yield the associated heats (Figure 7b and d). Control experiments were also performed by adding identical amounts of neomycin B to the buffer solution devoid of substrate to determine the respective heats of dilution. At low ionic strength, the plot of heat exchanged versus ligand/substrate ratio was biphasic, indicating that the binding events in solution could be best described by two distinct sets of equilibria (Figure 7b). At higher ionic strength, however, a monophasic profile was obtained, which could be best described by a single set of binding equilibria (Figure 7d). The two plots were further processed to derive the corresponding values of association constant (K_a), binding enthalpy (ΔH_{obs}) and stoichiometry (N), which are summarized in Table 2.

The ITC results support a primary neomycin B binding site on the PPT with a relatively high affinity and a 1:1 stoichiometry at both high and low ionic strengths. A second set of equivalent binding sites, with a stoichiometry of 2.34, was only detected at low ionic strength. This is indicative of less specific interactions and correlates with the intermediate exchange processes observed by ^{1}H NMR upon adding a second equivalent of neomycin B. The affinities observed for specific neomycin B binding to the PPT_{wt} hybrid are consistent with those observed for specific sites characterized in other nucleic acid complexes (56). In addition, the sizeable contribution of electrostatic interactions to the stability of aminoglycoside binding can be readily appreciated from the reduction of two orders of magnitude (i.e. from $1.45 \times 10^7\,M^{-1}$ to $1.07 \times 10^5\,M^{-1}$) for the K_a of the primary site after raising ionic strength. In this direction, docking experiments involving aminoglycoside antibiotics and RNA stem-loops of the HIV-1 packaging signal have clearly demonstrated the preferential binding of these positively charged ligands to regions that present a high density of negative charges on the substrate surface (32).

Conclusions

The application of archetypical nucleic acid ligands as non-covalent probes provides valuable information not only on motifs capable of sustaining stable binding, but also on the nature of the specific interactions (31,32). The binding modes exhibited by the intercalating agents ethidium bromide and mitoxantrone are consistent with decreasing stacking stabilization in the PPT series, from duplex DNA to RNA:DNA hybrid to RNA duplex. The fact that the two hybrids displayed comparable affinities indicates that stacking interactions do not determine recognition specificity on the wild-type PPT. Similar conclusions can be drawn from the binding modes provided by the groove-binder distamycin A, which tracked very closely the typical narrowing of the minor groove in moving from a canonic B-type to an A-type double helix. This probe, however, revealed subtle differences in affinity between hybrid constructs, possibly reflecting effects of sequence and strand sense on groove geometry.

Considering that aminoglycoside ligands bind nucleic acid duplexes with an RNA:RNA > RNA:DNA >> DNA:DNA scale of binding affinities (56,57), the preferential interaction of neomycin B with the wild-type RNA:DNA hybrid provides important evidence regarding the determinants of PPT recognition. The fact that this non-covalent probe manifested greater affinity for the wild-type hybrid than for its duplex RNA analogue diminishes the significance of generic canonical A-form helical structure in determining binding specificity (56), and highlights the importance of helix plasticity in adapting favorable electronegative surfaces for ligand interactions (46). The structural context of such surfaces is determinant and is expected to assume a clearly unique form in the wild-type substrate, as shown by comparison with the swapped construct, which displayed moderate affinity similar to non-PPT hybrids (56). In the case of the weaker 5′ $(rA)_4$:$(dT)_4$ site, the observed interaction is consistent with the ability of poly(rA)/poly(dT) triplexes to support specific aminoglycoside binding (58). However, there are no reported

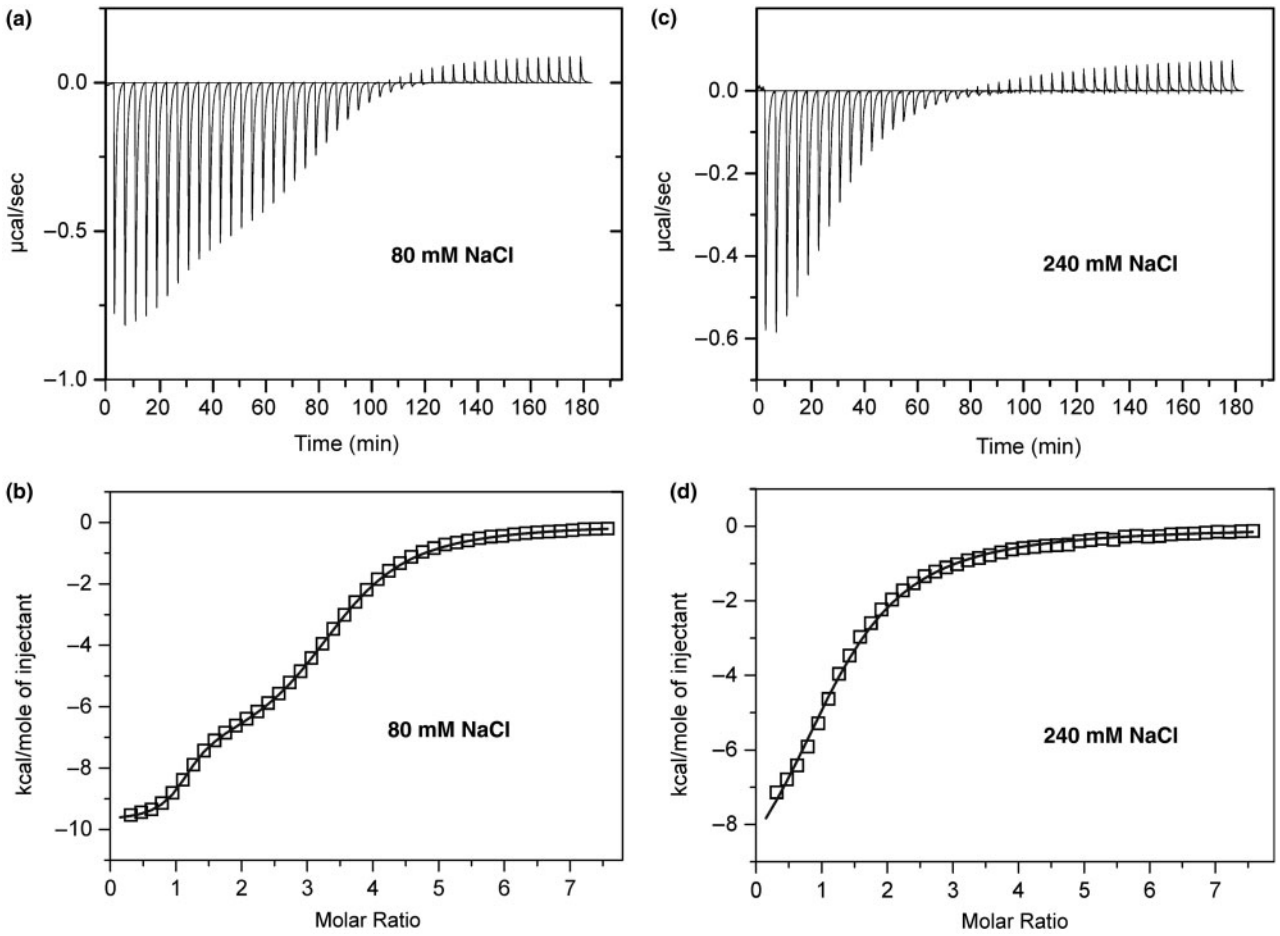

Figure 7. ITC titration of PPT_{wt} with neomycin B in 10 mM NaH_2PO_4/Na_2HPO_4 at pH 7.0 and 30°C. (**a**) ITC profile obtained at 80 mM NaCl; (**b**) integration of panel (a) and curve-fitting to a model including two sets of equivalents sites; (**c**) ITC profile obtained at 240 mM NaCl; (**d**) integration of panel (c) and curve-fitting to a model including one set of equivalent sites. The integrations in panels (b) and (**d**) were corrected for the heats of dilution from the titration of neomycin B into the respective buffer alone.

Table 2. Thermodynamic characteristics obtained by ITC of the wild-type PPT construct with neomycin B at 30°C

Salt conditions	80 mM NaCl	240 mM NaCl
T (°C)	30.0	30.0
N_1	1.09 ± 0.0075	1.25 ± 0.025
K_1 (10^5/M)	145 ± 10	1.07 ± 0.050
ΔH_1 (kcal/mol)	-9.70 ± 0.027	-1.11 ± 0.029
$T\Delta S_1$ (kcal/mol)	−2.94	−4.07
N_2	2.34 ± 0.0063	NA
K_2 (10^5/M)	2.76 ± 0.037	NA
ΔH_2 (kcal/mol)	-7.47 ± 0.036	NA
$T\Delta S_2$ (kcal/mol)	0.073	NA

NA: not applicable.

precedents for aminoglycoside interactions with RNA:DNA hybrid structures in the absence of bulges, mispaired bases, or other obvious structural anomalies, as in the PPT-U3 junction.

With its flexible backbone and polycationic character, neomycin B mimics the binding properties of basic peptides (46) and thus can indirectly provide insight into the mechanism of RT binding. The only available structure of an RT•PPT complex has the hybrid substrate placed in a ~60 Å cleft of the enzyme with numerous intermolecular contacts distributed along its length (PDB ID: 1HYS) (17). Considering that the same cleft is employed to bind any non-PPT RNA:DNA duplex formed during reverse transcription, it is not clear how this diffuse set of molecular contacts may translate into stringent substrate recognition. Unfortunately, in the high-resolution structure, the RNase H domain of RT was not positioned over the PPT-U3 junction, precluding identification of structural elements that might promote specific recognition. The non-covalent probe neomycin B clearly points toward the U3 junction and 5′ $(rA)_4$:$(dT)_4$ tract as favorable sites for preferential protein interactions driving recognition. The fact that the spacing between these PPT sites coincides closely with the distance between the RNase H active site and thumb subdomain of RT supports a requirement for proper matching between cognate structures as an additional element of recognition specificity. The results presented here provide strong experimental support to the proposed map of RT-PPT contacts shown in Figure 1.

Finally, the absence of probe binding in the region between the PPT-U3 junction and 5′ $(rA)_4$:$(dT)_4$ tract indicates that the corresponding cleft residues between

the RNase H domain and thumb subdomain play no significant role in specific substrate recognition. This observation implies that these domains may function as discrete binding units in the context of a putative bifunctional ligand, such as RT. The widely different binding modes exhibited by the substrate sites with the monofunctional probe neomycin B suggest a scenario in which the initial binding of either of these domains to the high-affinity site on the PPT-U3 junction could be followed by subsequent binding of the remaining domain to the low-affinity site on the 5′ $(rA)_4$:$(dT)_4$ tract. The fact that the second binding event is a unimolecular rather than a bimolecular process would compensate for the weaker and less specific nature of the interactions sustained by the 5′ $(rA)_4$:$(dT)_4$ tract. The possibility that the interplay between these binding events may mediate the orientation of RT onto the PPT substrate at different stages of the RT process will be the object of future investigations.

SUPPLEMENTARY DATA

Supplementary Data are available at NAR Online.

ACKNOWLEDGEMENTS

This research was funded by the National Institutes of Health (GM59107 to J.P.M. and GM643208 to D.F.) and by the National Science Foundation (CHE-0439067 to D.F.). R.G.B. is a NIST/NIH NRC postdoctoral fellow. S.F.J.L.G. was supported by the intramural research program of the National Cancer Institute, National Institutes of Health. Funding to pay the Open Access publication charges for this article was provided by NIH GM643208 to D.F.

Conflict of interest statement. Certain commercial equipment, instruments, and materials are identified in this paper in order to specify the experimental procedure. Such identification does not imply recommendation or endorsement by the National Institute of Standards and Technology, nor does it imply that the material or equipment identified is necessarily the best available for the purpose.

REFERENCES

1. Champoux,J.J. (1993) Roles of ribonuclease H in reverse transcription. In Skalka,A.M. and Goff,S.P. (eds), *Reverse transcriptase*, Cold Spring Harbor Laboratory Press, Cold Spring Harbor, NY, pp. 103–117.
2. Telesnitsky,A. and Goff,S.P. (1997) Reverse transcriptase and the generation of retroviral DNA. In Coffin,J.M., Hughes,S.H. and Varmus,H.E. (eds), *Retroviruses*, Cold Spring Harbor Laboratory Press, Cold Spring Harbor, NY. pp. 121–160.
3. Rausch,J.W. and Le Grice,S.F. (2004) 'Binding, bending and bonding': polypurine tract-primed initiation of plus-strand DNA synthesis in human immunodeficiency virus. *Int. J. Biochem. Cell Biol.*, **36**, 1752–1766.
4. Pillay,D., Taylor,S. and Richman,D.D. (2000) Incidence and impact of resistance against approved antiretroviral drugs. *Rev. Med. Virol.*, **10**, 231–253.
5. Johnson,V.A., Brun-Vezinet,F., Clotet,B., Kuritzkes,D.R., Pillay,D., Schapiro,J.M. and Richman,D.D. (2006) Update of the drug resistance mutations in HIV-1: Fall 2006. *Top HIV Med.*, **14**, 125–130.
6. Ren,J. and Stammers,D.K. (2004) HIV reverse transcriptase structures: designing new inhibitors and understanding mechanisms of drug resistance. *Trends Pharm. Sci.*, **26**, 4–7.
7. Pullen,K.A. and Champoux,J.J. (1990) Plus-strand origin for human immunodeficiency virus type 1: implications for integration. *J. Virol.*, **64**, 6274–6277.
8. Huber,H.E. and Richardson,C.C. (1990) Processing of the primer for plus strand DNA synthesis by human immunodeficiency virus 1 reverse transcriptase. *J. Biol. Chem.*, **265**, 10565–10573.
9. Wohrl,B.M. and Moelling,K. (1990) Interaction of HIV-1 ribonuclease H with polypurine tract containing RNA-DNA hybrids. *Biochemistry*, **29**, 10141–10147.
10. Powell,M.D. and Levin,J.G. (1996) Sequence and structural determinants required for priming of plus-strand DNA synthesis by the human immunodeficiency virus type 1 polypurine tract. *J. Virol.*, **70**, 5288–5296.
11. Arnott,S., Chandrasekaran,R., Millane,R.P. and Park,H.S. (1986) DNA-RNA hybrid secondary structures. *J. Mol. Biol.*, **188**, 631–640.
12. Fedoroff,O., Salazar,M. and Reid,B.R. (1993) Structure of a DNA:RNA hybrid duplex. Why RNase H does not cleave pure RNA. *J. Mol. Biol.*, **233**, 509–523.
13. Lane,A.N., Ebel,S. and Brown,T. (1993) NMR assignments and solution conformation of the DNA.RNA hybrid duplex d(GTGAACTT).r(AAGUUCAC). *Eur. J. Biochem.*, **215**, 297–306.
14. Horton,N.C. and Finzel,B.C. (1996) The structure of an RNA/DNA hybrid: a substrate of the ribonuclease activity of HIV-1 reverse transcriptase. *J. Mol. Biol.*, **264**, 521–533.
15. Fedoroff,O.Y., Ge,Y. and Reid,B.R. (1997) Solution structure of r(gaggacug):d(CAGTCCTC) hybrid: implications for the initiation of HIV-1 (+)-strand synthesis. *J. Mol. Biol.*, **269**, 225–239.
16. Kopka,M.L., Lavelle,L., Han,G.W., Ng,H.L. and Dickerson,R.E. (2003) An unusual sugar conformation in the structure of an RNA/DNA decamer of the polypurine tract may affect recognition by RNase H. *J. Mol. Biol.*, **334**, 653–665.
17. Sarafianos,S.G., Das,K., Tantillo,C., Clark,A.D.,Jr, Ding,J., Whitcomb,J.M., Boyer,P.L., Hughes,S.H. and Arnold,E. (2001) Crystal structure of HIV-1 reverse transcriptase in complex with a polypurine tract RNA:DNA. *EMBO J.*, **20**, 1449–1461.
18. Kvaratskhelia,M., Budihas,S.R. and Le Grice,S.F. (2002) Pre-existing distortions in nucleic acid structure aid polypurine tract selection by HIV-1 reverse transcriptase. *J. Biol. Chem.*, **277**, 16689–16696.
19. Rausch,J.W., Qu,J., Yi-Brunozzi,H.Y., Kool,E.T. and Le Grice,S.F. (2003) Hydrolysis of RNA/DNA hybrids containing nonpolar pyrimidine isosteres defines regions essential for HIV type 1 polypurine tract selection. *Proc. Natl Acad. Sci. USA*, **100**, 11279–11284.
20. Lener,D., Kvaratskhelia,M. and Le Grice,S.F. (2003) Nonpolar thymine isosteres in the Ty3 polypurine tract DNA template modulate processing and provide a model for its recognition by Ty3 reverse transcriptase. *J. Biol. Chem.*, **278**, 26526–26532.
21. Dash,C., Rausch,J.W. and Le Grice,S.F. (2004) Using pyrrolo-deoxycytosine to probe RNA/DNA hybrids containing the human immunodeficiency virus type-1 3′ polypurine tract. *Nucleic Acids Res.*, **32**, 1539–1547.
22. Dash,C., Yi-Brunozzi,H.Y. and Le Grice,S.F. (2004) Two modes of HIV-1 polypurine tract cleavage are affected by introducing locked nucleic acid analogs into the (-) DNA template. *J. Biol. Chem.*, **279**, 37095–37102.
23. Yi-Brunozzi,H.Y. and Le Grice,S.F. (2005) Investigating HIV-1 polypurine tract geometry via targeted insertion of abasic lesions in the (-)-DNA template and (+)-RNA primer. *J. Biol. Chem.*, **280**, 20154–20162.
24. Aleksandrov,M.L., Gall,L.N., Krasnov,V.N., Nikolaev,V.I., Pavlenko,V.A. and Shkurov,V.A. (1984) Extraction of ions from solutions under atmospheric pressure: a method of mass spectrometric analysis of bioorganic compounds. *Doklady Akademii Nauk.*, **277**, 379–383.
25. Yamashita,M. and Fenn,J.B. (1984) Electrospray ion source. Another variation on the free-jet theme. *J. Phys. Chem.*, **88**, 4671–4675.

26. Comisarow,M.B. (1978) Signal modeling for ion cyclotron resonance. *J. Chem. Phys.*, **69**, 4097–4104.
27. Marshall,A.G., Hendrickson,C.L. and Jackson,G.S. (1998) Fourier transform ion cyclotron resonance mass spectrometry: a primer. *Mass Spectrom. Rev.*, **17**, 1–35.
28. Ganem,B., Li,Y.T. and Henion,J.D. (1991) Detection of non-covalent receptor-ligand complexes by mass spectrometry. *J. Am. Chem. Soc.*, **113**, 6294–6296.
29. Loo,J.A. (1997) Studying noncovalent protein complexes by electrospray ionization mass spectrometry. *Mass Spectrom. Rev.*, **16**, 1–23.
30. Daniel,J.M., Friess,S.D., Rajagopalan,S., Wendt,S. and Zenobi,R. (2002) Quantitative determination of noncovalent binding interactions using soft ionization mass spectrometry. *Int. J. Mass Spectrom. Ion Proc.*, **216**, 1–27.
31. Turner,K.B., Hagan,N.A. and Fabris,D. (2006) Inhibitory effects of archetypical nucleic acid ligands on the interactions of HIV-1 nucleocapsid protein with elements of Ψ-RNA. *Nucleic Acids Res.*, **34**, 1305–1316.
32. Turner,K.B., Hagan,N.A., Kohlway,A. and Fabris,D. (2006) Mapping noncovalent ligand binding to stemloop domains of the HIV-1 packaging signal by tandem mass spectrometry. *J. Am. Soc. Mass Spectrom.*, **17**, 1401–1411.
33. Hagan,N. and Fabris,D. (2003) Direct mass spectrometric determination of the stoichiometry and binding affinity of the complexes between HIV-1 nucleocapsid protein and RNA stem-loops hairpins of the HIV-1 Ψ-recognition element. *Biochemistry*, **42**, 10736–10745.
34. Hagan,N.A. and Fabris,D. (2007) Dissecting the protein-RNA and RNA-RNA interactions in the nucleocapsid-mediated dimerization and isomerization of HIV-1 stemloop 1. *J. Mol. Biol.*, **365**, 396–410.
35. de Koning,L.J., Nibbering,N.M.M., van Orden,S.L. and Laukien,F.H. (1997) Mass selection of ions in a Fourier transform ion cyclotron resonance trap using correlated harmonic excitation fields (CHEF). *Int. J. Mass Spectrom. Ion Proc.*, **165/166**, 209–219.
36. Gauthier,J.W., Trautman,T.R. and Jacobson,D.B. (1991) Sustained off-resonance irradiation for collision-activated dissociation involving Fourier transform mass spectrometry. Collision-activated dissociation technique that emulates infrared multiphoton dissociation. *Anal. Chim. Acta*, **246**, 211–225.
37. Le Grice,S.F. and Gruninger-Leitch,F. (1990) Rapid purification of homodimer and heterodimer HIV-1 reverse transcriptase by metal chelate affinity chromatography. *Eur. J. Biochem.*, **187**, 307–314.
38. Probst,C.L. and Perun,T.J. (1992) In *Nucleic Acid Targeted Drug Design*. Marcel Dekker, Inc., New York, NY.
39. Chaires,J.B. (1998) Drug-DNA interactions. *Curr. Opin. Struct. Biol.*, **8**, 314–320.
40. Hermann,T. (2003) Chemical and functional diversity of small molecule ligands for RNA. *Biopolymers*, **70**, 4–18.
41. Griffey,R.H., Hofstadler,S.A., Sannes-Lowery,K.A., Ecker,D.J. and Crooke,S.T. (1999) Determinants of aminoglycoside-binding specificity for rRNA by using mass spectrometry. *Proc. Natl Acad. Sci. USA*, **96**, 10129–10133.
42. Maddaford,S.P., Motamed,M., Turner,K.B., Choi,M.S.K., Ramnauth,J., Rakhit,S., Hudgins,R.R., Fabris,D. and Johnson,P.E. (2004) Identification of a novel non-carbohydrate molecule that binds to the ribosomal A-site RNA. *Bioorg. Med. Chem. Lett.*, **14**, 5987–5990.
43. Krugh,T.R. and Reinhardt,C.G. (1975) Evidence for sequence preferences in the intercalative binding of ethidium bromide to dinucleoside monophosphates. *J. Mol. Biol.*, **97**, 133–162.
44. Hardwick,J.M., von Sprecken,R.S., Yielding,K.L. and Yielding,L.W. (1984) Ethidium binding sites on plasmid DNA determined by photoaffinity labeling. *J. Biol. Chem.*, **259**, 11090–11097.
45. Kopka,M.L., Yoon,C., Goodsell,D., Pjura,P. and Dickerson,R.E. (1985) The molecular origin of DNA-drug specificity in netropsin and distamycin. *Proc. Natl Acad. Sci. USA*, **82**, 1376–80.
46. Busscher,G.F., Rutjes,F.P.J.T. and van Delft,F.L. (2005) 2-Deoxystreptamine: central scaffold of aminoglycoside antibiotics. *Chem. Rev.*, **105**, 775–791.
47. Hunt,D.F., Shabanowitz,J., Yates,J.R.,3rd, Zhu,N.Z., Russell,D.H. and Castro,M.E. (1987) Tandem quadrupole Fourier transform mass spectrometry of oligopeptides and small proteins. *Proc Natl Acad. Sci. USA*, **84**, 60–63.
48. McLafferty,F.W. (1981) Tandem mass spectrometry. *Science*, **214**, 280–287.
49. Honig,B. and Nicholls,A. (1995) Classical electrostatics in biology and chemistry. *Science*, **268**, 1144–1149.
50. Yi-Brunozzi,H.Y., Brinson,R.G., Brabazon,D.M., Lener,D., Le Grice,S.F.J. and Marino,J.P. (2008) High-resolution NMR analysis of the conformations of native and base analog substituted retroviral and LTR-retrotransposon PPT primers. *Chem. Biol.*, in press.
51. Gorshkova,II., Rausch,J.W., Le Grice,S.F. and Crouch,R.J. (2001) HIV-1 reverse transcriptase interaction with model RNA-DNA duplexes. *Anal. Biochem.*, **291**, 198–206.
52. Bohlayer,W.P. and DeStefano,J.J. (2006) Tighter binding of HIV reverse transcriptase to RNA-DNA versus DNA-DNA results mostly from interactions in the polymerase domain and requires just a small stretch of RNA-DNA. *Biochemistry*, **45**, 7628–7638.
53. Abbondanzieri,E.A., Bokinsky,G., Rausch,J.W., Zhang,J., Le Grice,S.F.J. and Zhuang,X. Dynamic binding orientations determine the enzymatic activity of HIV reverse transcriptase. *Nature*, in press.
54. Perozzo,R., Folkers,G. and Scapozza,L. (2004) Thermodynamics of protein-ligand interactions: history, presence, and future aspects. *J. Recept. Sign. Trans.*, **24**, 1–52.
55. Haq,I., Jenkins,T.C., Chowdhry,B.Z., Ren,J. and Chaires,J. (2000) Parsing free energies of drug-DNA interactions. *Meth. Enz.*, **323**, 373–405.
56. Barbieri,C.M., Li,T.K., Guo,S., Wang,G., Shallop,A.J., Pan,W., Yang,G., Gaffney,B.L., Jones,R.A. and Pilch,D.S. (2003) Aminoglycoside complexation with a DNA•RNA hybrid duplex: the thermodynamics of recognition and inhibition of RNA processing enzymes. *J. Am. Chem. Soc.*, **125**, 6469–6477.
57. Li,T.K., Barbieri,C.M., Lin,H.C., Rabson,A.B., Yang,G., Fan,Y., Gaffney,B.L., Jones,R.A. and Pilch,D.S. (2004) Drug targeting of HIV-1 RNA.DNA hybrid structures: thermodynamics of recognition and impact on reverse transcriptase-mediated ribonuclease H activity and viral replication. *Biochemistry*, **43**, 9732–9742.
58. Arya,D.P., Coffee,R.L.Jr and Charles,I. (2001) Neomycin-induced hybrid triplex formation. *J. Am. Chem. Soc.*, **123**, 11093–11094.